Manuscript prepared for Geosci. Instrum. Method. Data Syst.
with version 5.0 of the LaTeX class copernicus.cls.
Date: 28 May 2013

Optimal design of a climatological network: beyond practical considerations

G. S. Mauger[1], K. A. Bumbaco[2], G. J. Hakim[3], and P. W. Mote[4]

[1]Climate Impacts Group, University of Washington, Box 355674, Seattle, WA 98195-5672, USA
[2]Office of the Washington State Climatologist, University of Washington, Box 355672, Seattle, WA 98195-5672, USA
[3]Department of Atmospheric Sciences, Box 351640, University of Washington, Seattle, WA 98195-1640, USA
[4]College of Earth, Ocean, and Atmospheric Sciences, 104 CEOAS Admin Building, Oregon State University, Corvallis, OR 97331, USA

Correspondence to: G. S. Mauger (gmauger@uw.edu)

Abstract. Station locations in existing environmental networks are typically chosen based on practical constraints such as cost and accessibility, while unintentionally overlooking the geographical and statistical properties of the information to be measured. Ideally, such considerations should not take precedence over the intended monitoring goal of the network: the focus of network design should be to adequately sample the quantity to be observed.

Here we describe an optimal network design technique, based on ensemble sensitivity, that objectively locates the most valuable stations for a given field. The method is computationally inexpensive and can take practical constraints into account. We describe the method, along with the details of our implementation, and present example results for the US Pacific Northwest, based on the goal of monitoring regional annual-mean climate. The findings indicate that optimal placement of observing stations can often be highly unintuitive, thus emphasizing the importance of objective approaches. Although at coarse scales the results are generally consistent, sensitivity tests show important differences in the results, especially at smaller spatial scales. These uncertainties could be reduced with improvements in datasets and improved estimates of the measurement error. We conclude that the method is best suited for identifying general areas within which observations should be focused, and suggest that the approach could serve as a valuable complement to land surveys and expert input in designing new environmental observing networks.

1 Introduction

Environmental observing networks are established for a wide variety of purposes, ranging from short-term weather forecasting to monitoring ecosystem change. A compromise between scientific and practical considerations (e.g., site accessibility, cost, land ownership) usually governs the placement of stations, though practical considerations often have a greater influence on the final station locations. Historically, station site selection has typically been made subjectively, which suggests that the goals for the network are not met optimally or cost effectively. Theories for optimal observing networks have matured to the point where an objective cost-benefit analysis can be considered when creating, augmenting, or revising an observing network. Objectivity is important because results show that optimally selected station locations often do not follow from intuition. Here we describe a flexible ensemble-based network-design algorithm that incorporates measurement error and can account for practical considerations such as accessibility of the site and land ownership.

An example of an observing network is the cooperative observer (COOP) weather network, which was established in the 19th century and remains the primary legacy network for climate monitoring in the United States. Since the COOP network relies heavily on volunteer observers, nearly all stations are situated in inhabited areas, and stations consequently tend to cluster in lower elevations. Installation and annual upkeep is more costly for remote stations, and these locations are often overlooked. For areas with complex terrain such as the western United States, low-lying networks near population centers do not accurately represent the climate in adjacent mountainous areas, especially for precipitation (Dabberdt and Schlatter, 1996). Variations in wind and sun exposure, cold air pooling in mountain valleys, and coastal fog are just a few examples of common weather occurrences that can result in sharp climate distinctions across fairly short distances (e.g., Lundquist and Cayan, 2007; Abatzoglou et al., 2009). As a result, it is possible for closely spaced stations to sample vastly different climates, or conversely, for two distant stations to be highly correlated and hence largely redundant. Prior studies have confirmed this (e.g., Fujioka, 1986; Hargrove et al., 2003), showing that uniformly spaced stations do not provide an advantage over those that are optimally placed. Fujioka (1986), for example, found that the optimal station locations were non-intuitive, and had 15 times less normalized error than the gridded locations in representing fire weather variables in southern CA.

Clearly, methods are needed that can help objectively identify compromises between scientific and practical considerations when designing and augmenting an observing network. By optimally determining the most valuable observation sites, the utility of a network can be maximized and the cost minimized as redundancy and guesswork in station placement is reduced.

2 Methods

2.1 Ensemble Sensitivity

The ensemble sensitivity approach to network design is based on the idea of adaptive (or targeted) observations (e.g., Bergot et al., 1999; Morss et al., 2001; Bishop and Toth, 1999). Although the criteria are quite different, the same principles can be applied to the development of a fixed network for long-term monitoring. The problem centers on improving estimates of a scalar measure of interest, or "metric", J. Applied to network design, the method (e.g., Khare and Anderson, 2006; Ancell and Hakim, 2007; Huntley and Hakim, 2010) works by iteratively finding sites that explain the most variance of a given climate field while accounting for the variance explained by previous "stations" selected (hereafter, the term "station" is used to refer to the optimal observing locations identified in the ensemble sensitivity approach). Finding the first station is relatively straightforward: it consists of identifying the point with the highest correlation with the metric while also maximizing the ratio of that correlation to the measurement error. Locating the second station is more difficult because the choice must account for the variance already explained by the first station. As discussed below, this is accomplished by using the Kalman update equation to adjust the sampled values at each grid point. The process then repeats: a new station is chosen, and the ensemble sample is adjusted to account for the new information that this station provides. With each chosen station, the variance in the data decreases according to the variance explained by the previous stations. At some point, very little additional variance is gained by identifying new stations, or alternatively, the remaining variance becomes indistinguishable from the noise. This point is reached when no new information is gained by adding stations beyond the number already identified (in Sect. 2.5 we describe our bootstrap approach to approximating this threshold). Note that the method is general: no specific time-step, variables, or spatial configuration is required – this is a key strength of the approach. A brief description of the algorithm follows.

In ensemble sensitivity analysis, different samples of the state of the system ($\mathbf{x}$) are used to develop statistics that relate changes in the state of the system to changes in a particular metric of interest (J). Using a gridded "truth" field as a proxy for observations, an optimally located observation is thus defined as the grid point that contributes most to the variance in J, our metric of interest. We accomplish this by calculating the change in the variance of J ($\Delta\sigma_J^2$) for each grid point, and identifying the grid point for which this change is maximized. By using anomalies in the state of the system ($\mathbf{x}$) and a first-order Taylor expansion of J, Ancell and Hakim (2007) show that $\Delta\sigma_J^2$ can be

rewritten as follows:

$$\Delta\sigma_J^2 = \sigma_{J,i-1}^2 - \sigma_{J,i}^2 \tag{1}$$

$$= \left[\frac{\partial J}{\partial \mathbf{x}}\right]^T \mathbf{K}_i \mathbf{H}_i \mathbf{B}_{i-1} \left[\frac{\partial J}{\partial \mathbf{x}}\right] \tag{2}$$

$$\mathbf{K}_i = \mathbf{B}_{i-1}\mathbf{H}_i^T \mathbf{E}_i^{-1} \tag{3}$$

$$\mathbf{E}_i = \mathbf{H}_i \mathbf{B}_{i-1} \mathbf{H}_i^T + R^2 \tag{4}$$

where i refers to the ith iteration of the algorithm, $\mathbf{B}_{i-1}$ is the prior error covariance of $\mathbf{x}$, $\mathbf{E}_i$ is the "innovation error covariance", and R^2 is the measurement error, which includes both instrument and "representativeness" error (i.e., error associated with sub-grid variability). $\mathbf{H}_i$ is a linearized observation operator, which maps the state of the system ($\mathbf{x}$) to an observation of interest. In Eq. (2), the change in the error covariance upon selection of the ith station is estimated using the Kalman gain (Eq. 3; Hamill, 2006; Kalman, 1960) associated with the new observation.

As discussed above, the selection of the ith station is conditioned on the variance explained by the previous $(i-1)$ stations. In matrix form, this conditional adjustment is applied using the classic Kalman update equation for the covariance matrix ($\mathbf{B}_i = (\boldsymbol{I} - \mathbf{K}_i\mathbf{H}_i)\,\mathbf{B}_{i-1}$). The matrix implementation, however, has two principle disadvantages: (1) it can be numerically unstable, and (2) it is computationally expensive. As a result, we instead use the square root implementation of the Kalman update equation, as follows:

$$\Delta\sigma_J^2 = \frac{\mathrm{cov}(J, x_{m,i})^2}{\sigma_{x_{m,i}}^2 + R_m^2} \tag{5}$$

$$x_{m,i} = x_{m,i-1} - \beta \left(\frac{\mathrm{cov}(x_{m,i-1}, x_{\mathrm{stn},i-1})}{\sigma_{x_{\mathrm{stn},i-1}}^2 + R_m^2} \right) x_{\mathrm{stn},i-1} \tag{6}$$

$$\beta = \frac{1}{1 + \sqrt{\frac{R_m^2}{\sigma_{x_{\mathrm{stn},i-1}}^2 + R_m^2}}} \tag{7}$$

where x_m refers to the time series for an arbitrary grid point, x_{stn} refers to the time series for the ith selected station, and β is a term that results from the conversion from matrix to square root form (Potter, 1964). These simplified equations arise from the fact that, in serial processing (i.e., the square root implementation), $\mathbf{H}_i$ is simply a vector that extracts the mth grid point of $\mathbf{x}$ (i.e., $\mathbf{H}_i = [0, 0, \ldots, 1, \ldots, 0]$; see Huntley and Hakim, 2010).

Although perhaps less elegant than in their matrix form, these equations help illustrate the logic behind the approach. First, note that Eq. (5) very closely resembles the square of the correlation between J and the time series at each grid point, the only differences being a missing constant (σ_J^2) and an added error term (R^2) in the denominator. At each step in the calculation, the optimal station is selected by identifying the grid point for which $\Delta\sigma_J^2$ is maximized. The error term serves to promote areas where the correlation with J is large compared to the measurement uncertainty. Second, note that Eq. (6) essentially uses an ordinary least squares regression, scaled by β, to adjust

the sample values at each grid point (x_m). The conditional adjustment is thus achieved by removing that portion of the variance in x_m that can be reproduced using the time series of the selected station (x_{stn}). Finally, note that the parameter β is always between 0.5 and 1, and thus serves to reduce the adjustment to x_m, based on the proportion of grid cell variance to measurement uncertainty (R^2).

The approach we have described rests on several key assumptions. Specifically, the Kalman update equation is only optimal if the following conditions are met:

1. *Linear*: the approach involves a linearization about the time-averaged state.

2. *Gaussian*: the model state variables (and associated noise) are Gaussian in distribution.

These assumptions are discussed in Section 2.3 below.

2.2 Data

We apply the approach to the problem of monitoring regionally- and annually-averaged precipitation and temperature over the US Pacific Northwest (hereafter "PNW"), which we define to span the three states of Oregon, Washington, and Idaho (see Fig. 1). This is based loosely on the recent interest in improving climate monitoring across the US, as exemplified by the deployment of the Climate Reference Network (CRN) in the early 2000s. As we note above, although there are numerous observing stations throughout this region, the sampling is biased towards lower elevations and population centers, in all likelihood leaving important features of the regional climate unobserved. The purpose of the present exercise is thus to identify the locations where surface measurements would be most valuable, with regard to the goal of monitoring annual climate in the PNW. For simplicity we assume that we are designing the network from scratch and neglect practical considerations such as land ownership and access. The results thus identify the most valuable observing locations, irrespective of existing measurements or constraints on land use, access, etc. As discussed in the conclusions, the method can be easily adapted to incorporate such considerations.

In order to explore the sensitivity to the dataset used to define the stationary climate, we apply the method using three meteorological datasets listed in Table 1. PRISM (Daly et al., 2002) is created by gridding point observations and using an interpolation scheme that accounts for influences of terrain on climate including rain shadows, coastal effects, and temperature inversions. Annual temperature and precipitation data were obtained at 2.5 arc-minute (~ 4 km) resolution from the PRISM Climate Group website (www.prism.oregonstate.edu) for the years 1948–2011. Note that although PRISM data are available for 1895 to present, we chose to use only data from 1948 onward due to the greater station density in the latter part of the record. NARR (Mesinger et al., 2006) is an assimilated dataset covering North America from 1979 to present at a spatial resolution of 32 km. Data were obtained from the National Climatic Data Center (NCDC; http://nomads.ncdc.noaa.gov/). GHCN is an integrated and quality-assured database of land surface stations (Lawrimore et al., 2011; stations included in the present analysis are listed in Table 4). Daily data were quality controlled by

eliminating any temperature excursions that exceeded 5 standard devations of all daily measurements for a specific calendar month, and any daily precipitation measurements that exceeded 254 mm (10 inches). Annual averages of GHCN observations were compiled from daily data by requiring a minimum of 10 days to compute a monthly average and 9 months to compute an annual average – different choices for these thresholds did not substantially impact the results. The 181 stations with complete records for 1979–2011 were included in the analysis.

Before proceeding, we assess the extent to which the data satisfy the two assumptions listed in the previous section, which are necessary conditions for applying the ensemble sensitivity approach. The first assumption, linearity, is not an issue for our application: since we intend to model precipitation and temperature using distributed observations of precipitation and temperature, our model simply consists of an average and is therefore linear.

The assumption of Gaussian statistics is worth investigating in some depth, in particular with regard to precipitation, which – even at annual time scales – exhibits a distribution that is skewed toward larger values. Table 2 lists the statistics of temperature, raw precipitation, and tranformed precipitation data, showing the range of each statistic over all grid points. The transformed precipitation was created by remapping the observed cumulative distribution of precipitation to that of a normal distribution (by matching quantiles). To preserve the spatial variability in precipitation, the width of the normal distribution was scaled to match the variance of the observations. The transformation was performed separately for each grid cell since, although lumping all of the data together would improve sampling, it would not guarantee Gaussian statistics at each point. As can be seen in Table 2, the main impact of the precipitation transform is to eliminate any skewness in the data, though it is notable that the raw precipitation data is very nearly Gaussian as well. For this reason, our default in the calculaions below is to use raw precipitation, though we note the impact of using transformed precipitation in the sensitivity tests discussed below.

2.3 Measurement Error

The method takes into account measurement error (denoted R^2 in Eq. 3) resulting primarily from instrumental error and representativeness error, the latter being the error due to the fact that variability exists at the subgrid scale. Although in principle these quantities can be estimated, in practice such estimates are quite uncertain. In the present study, we use an empirically-based estimate of the error variance in *daily* observations of surface temperature used by the European Centre for Medium-Range Weather Forecasting (ECMWF), of $3.6\,\mathrm{K}^2$. Assuming an autocorrelation time scale of 5 days, we obtain an *annual* error variance of about $0.05\,\mathrm{K}^2$ for annual average temperature. A constant value for R^2 is applied to all grid cells. Since measurements of precipitation are not generally assimilated in weather forecasting, there does not exist a similar estimate for the appropriate error variance in precipitation. As a result, we estimate the error variance for precipitation by simply rescaling the value used for temperature using the ratio of the variance in precipitation to the

variance in temperature, and accounting for a precipitation autocorrelation time scale of 2 days instead of 5. This corresponds to an error variance of $\sim 3.6\,\%$ of the variance in precipitation at each grid cell and a mean error variance of $500\,\mathrm{mm}^2$ (for total annual precipitation). Note that this is an approximation, since precipitation measurements are subject to different and often greater errors than for temperature. However, such differences are likely far less than the span of the sensitivity tests for R^2, described below. Finally, note that in contrast with temperature, R^2 is scaled with the grid cell variance in precipitation, since using a constant error variance would bias the results in favor of wetter regions.

Since both estimates of R^2 are approximations, we perform two simple verifications: (1) using raw surface observations from two nearby stations, and (2) using a gridded estimate of representativeness error. Note that in both cases we are assuming that the magnitude of R^2 is dominated by the representativeness error – a good assumption given that propagating the error in daily measurements of temperature and precipitation gives an annual instrument error of about $0.0001\ \mathrm{K}^2$ and $0.01\ \mathrm{mm}^2$, respectively.

In the first approach we consider the mean-squared difference between two nearby observing stations – Sea-Tac airport (47.45° N, 122.3° W) and Kent COOP (47.4° N, 122.2° W) – for the overlapping time series spanning 1951–2011. The result is a value of $0.28\,\mathrm{K}^2$ for temperature and $7800\,\mathrm{mm}^2$ for precipitation. Our central estimate for R^2 at that location is $\sim 950\,\mathrm{mm}^2$ for precipitation (and, as with all grid cells, $0.05\,\mathrm{K}^2$ for temperature). Note that the distance between these two observing stations is 7.5 km, which is about twice the grid resolution of the PRISM dataset, making it likely that these numbers represent an overestimate of representativeness error

Our second approach to verifying the R^2 estimates from ECMWF is to use the 30 arc-second ($\sim$800 m resolution) climatologies available from PRISM to estimate the sub-grid variance in temperature and precipitation for each 2.5 arc-minute ($\sim$4 km) grid cell. This gives an estimate of the representativeness error that varies with each grid cell, with a median of $0.06\,\mathrm{K}^2$ for temperature and $600\,\mathrm{mm}^2$ for precipitation. The corresponding values from ECMWF are $0.05\,\mathrm{K}^2$ for temperature, and $375\,\mathrm{mm}^2$ for precipitation, indicating that as above, the ECMWF estimates are somewhat conservative but well within the range of our sensitivity tests, discussed below.

2.4 Sensitivity Tests

As the above discussion of measurement error highlights, several of the parameters used in applying the method are uncertain. Specifically, in addition to measurement error, the method may be sensitive to the choice of climate dataset, precipitation transform, the number of years included in the gridded data, the sample size (in years) for each calculation, and assumptions about the number of stations that the algorithm can meaningfully identify (i.e., as limited by sampling error). To address the sampling issues, we implemented a Monte Carlo routine in which the algorithm was run 50 000 times, using a different random sample of years for each iteration. The Monte Carlo approach

also addresses the question of noise limitations, since statistics can be obtained on the consistency of results between iterations (see discussion below). To test robustness to other parameters, we performed the following sensitivity tests: measurement error variance (R^2) was scaled by a factor ranging from 0.1 to 10, calculations were repeated for different climate datasets, precipitation transforms, sample sizes (ranging from 20 to 40 yrs), and years from which to draw samples (1948–1979 vs. 1980–2011).

3 Results and discussion

Figure 2 shows the best estimate of the optimal observing locations, obtained using the following choices of data and parameters:

- Metric (J): regionally averaged annual Temperature and Precipitation
- Dataset: PRISM
- Years: 1948–2011
- Sample size: 30 yr
- $R^2 = 0.05\,\mathrm{K}^2$ for temperature
- $R^2 = 3.6\,\%$ of the grid cell variance in precipitation
- Precipitation: raw data (not transformed)

In this section we discuss these results along with the results of our sensitivity tests, which evaluate the impact of varying the above parameters and assumptions.

We summarize the results by producing maps that show the frequency, among all Monte Carlo iterations, with which a grid point is selected in the top "N" stations, where "N" is chosen to correspond to some average total variance explained in regional temperature or precipitation. This accounts for sample variability while highlighting areas that are most likely to contribute optimally to monitoring regional climate. The result is a frequency value for each grid point, which can then be mapped as shown in Fig. 2. Since these frequency values are most meaningful in a relative sense – which grid cells have greater weightings than others – we display the percentile values of the grid cell weightings, which we consider more helpful for interpretation. For example, a point is assigned a 95^{th} percentile value if its *frequency value* – the fraction of Monte Carlo iterations in which it was selected in the top "N" points – is greater than or equal to that of 95 % of all other points. Finally, in this and subsequent maps stemming from gridded PRISM data, the results have been averaged from 2.5 arc-min (~ 4 km) resolution to 0.5 degree resolution. This smoothing is applied to aid in interpretation.

In order to choose "N" we look at the change in the variance explained as the calculation progresses – in other words, the percent of the variance in the metric (regional temperature or precipitation) that can be reproduced using a linear combination of the already-chosen stations. Table 3 lists the mean variance explained for both temperature and precipitation, for each additional station selection, for the results mapped in Fig. 2. As described in Sect. 2.2, the calculation proceeds by selecting stations that maximize the residual variance explained – in other words, that maximize the additional value lent by their selection. Table 3 illustrates that, due to high spatial autocorrelation across the region (in particular at annual time scales), the first station explains a majority of the variance, while subsequent stations account for progressively less of the residual variance. By summing the variance explained at each step we find that, on average, the top 3 stations in temperature and the top 2 in precipitation are sufficient to explain 95 % of the variance in the annual climate signal for the PNW. Similarly, to explain 99 % of the variance would require selection of the top 11 and 4 stations for temperature and precipitation, respectively. For simplicity, we only show results for the former (i.e., 95 % variance explained) in Fig. 2 and all subsequent figures. The results for different choices are qualitatively similar.

The results shown in Fig. 2 highlight several regions that are important for capturing the regional signal of climate variability. The results for temperature, for instance, highlight the central Snake River plain in Idaho, the mountains of northeast Oregon, and north-central Washington, among other regions (see Fig. 1 for a key to the geography of the region). For precipitation, the results are quite different, primarily highlighting the central Cascades, the Columbia gorge near Portland, the southeastern slopes of the Olympic mountains in Washington, and certain parts of the coast of Oregon. Notably, the optimal locations for monitoring temperature are almost entirely east of the Cascade mountains, while the opposite is true for the optimal observing locations identified for precipitation. In addition, some of the results are quite unintuitive. For instance, while it makes sense that precipitation monitoring will maximize signal to noise on the substantially wetter western slopes of the Cascade mountains, it is not intuitively obvious that the central Cascade mountains are more appropriate than any other portion of this mountain range, nor is it clear why the even wetter western slopes of the Olympic mountains are hardly highlighted at all.

Figure 3 shows a comparison of results obtained from the three datasets: GHCN, NARR, and PRISM. In order to perform a direct comparison, NARR and PRISM data were only used for the grid points that correspond most closely to the location of each GHCN station, and all datasets applied to the years 1979–2011 only, with a sample size of 20 yr for each calculation. The R^2 values applied to each case were identical. Note that this is not a perfect comparison, since point measurements (i.e., GHCN) are different from grid-cell averages (NARR, 32 km resolution; PRISM, $\sim$ 4 km resolution).

The rank correlations between the GHCN results and each gridded dataset are shown in the upper right-hand corner of each map. Since disagreement among adjacent stations could confound the results, we calculated correlations by first averaging the point results for each dataset onto a 0.5

degree grid. Point correlations (not shown) were significant but substantially lower than their gridded counterparts. We use rank correlations because the results are highly skewed, causing standard correlations to be disproportionately affected by a small number of points. Since our emphasis in this work is on the relative rankings among grid points, we deem the rank correlations a better measure of similarities among the results. Standard correlations also revealed significant positive correlations, but nonetheless lower values.

A number of observations can be made from these results. First, at coarse scales (i.e., the broad regions highlighted) there is good agreement among the three datasets. Second, PRISM and GHCN bear the greatest similarities, a fact which is perhaps not surprising given that PRISM is essentially a regridding of surface observations. Third, although the general picture remains consistent between datasets, the specific rankings can differ substantially (as reflected in the correlations). Since the three agree well at coarser spatial scales, this suggests that the discrepancies are primarily in the treatment of climate variations across smaller scales. We thus conclude that, until well-validated improvements in datasets become available, the results are best viewed as defining broad regions within which to focus efforts. Based on this comparison, Fig. 2 and all subsequent results are shown using the PRISM dataset, averaged to 0.5 degree resolution (i.e., calculations are performed at the native PRISM resolution of ~ 4 km, then averaged to 0.5 degree resolution for presentation).

A primary advantage of our approach is that it is objective, and that it is therefore capable of highlighting non-intuitive but nonetheless optimal observing locations. However, implementation of the method does entrain a number of important subjective decisions, as highlighted at the beginning of this section. Figures 4 and 5 show how the results are affected by varying the parameters chosen for the calculation. Specifically, we test for the influence of variations in the sample size (20 vs. 40 yr), the years from which to draw a sample (1948–1979 vs. 1980–2011), and the value for the total error variance (R^2; 10 times smaller vs 10 times larger than our central estimate) in temperature (Fig. 4) and precipitation (Fig. 5). Note that changing the values of R^2 changes the number of stations ("N") needed to achieve 95 % variance explained – these were adjusted accordingly in the maps showing sensitivity to R^2. Note, also, that we do not consider variations in the metric (J) – this would by definition alter the results, but would not inform our question regarding the robustness of the method.

Overall, as with Fig. 3, these results show broad consistencies across different parameter values, highlighting similar areas for monitoring despite large variations in parameters. Precipitation results appear to be much more robust than those for temperature. For both variables, the results are largely insensitive to the choice of sample size, but indicate a fair sensitivity to the choice of years sampled and, in particular, to R^2. The magnitude of R^2 impacts the extent to which explanatory power is balanced by the ratio of signal-to-noise: small values for R^2 favor areas that correlate best with the regional signal, while large values of R^2 favor areas with higher variance. Even in the case of R^2, it is notable that the dominant regions highlighted nearly always correspond to regions that are also highlighted in Fig. 2.

For precipitation, we also considered the influence of holding R^2 constant across the domain and of applying a Gaussian transform to the precipitation results. Although not shown, the results using transformed precipitation correlated highly ($r = 0.85$; as above, we computed rank correlations after regridding to 0.5 degree) with the original results, indicating that at annual time scales the raw data are sufficiently Gaussian. Results obtained by using constant measurement error were less similar ($r = 0.57$), with differences largely resulting from the greater influence of regions west of the Cascade mountains. These differences are anticipated, since there are sharp changes in precipitation across the region, and a constant R^2 will favor regions with greater accumulation.

4 Conclusions

The ensemble sensitivity approach provides an objective method for allocating resources to develop an observational network. It allows for rapid evaluation of different metrics, and requires only a climatological sample. Since the utility of each observation is maximized, optimal placement ensures an efficient use of resources. There are two salient features to the approach: (1) stations are selected based on a compromise between their correlation with the metric and the ratio of signal-to-noise, and (2) new selections are constrained to minimize redundancy by maximizing the *additional* variance explained.

We present an example in which the goal is to optimally monitor regional climate in the US Pacific Northwest. Our analysis suggests that this goal can be achieved with 5 to 10 optimally placed stations. We find that station placement is not intuitive, highlighting the importance of employing objective methods for network design. Note that this information can be used in one of two ways: (1) install only 5-10 new observing stations instead of the total number planned, or (2) pursue other monitoring goals (e.g., monitoring local climate, seasonal climate, or probability of extremes).

Sensitivity tests indicate that the results are robust to the choice of sample size and time period analyzed, but that there are important differences resulting from the choice of dataset and assumed measurement error (R^2). Sensitivity to R^2 is fairly strong, but in general does not result in the identification of new regions for monitoring. Differences among datasets are likely partially attributable to differences in spatial resolution and the distinction between point measurements and grid cell averages. However, it is also likely that these differences represent real differences in the modeled covariability of temperature and precipitation across the region. Fortunately, the differences among datasets largely result from small spatial scale distinctions between each: the broad-scale patterns are consistent. Since important differences do exist, we conclude that until an improved dataset becomes available, the method is best used to identify general areas in which to locate stations. In practice, this is unlikely to be a limitation, since siting decisions at local scales are dominated by practical constraints such as land ownership, access, etc.

The example we present pertains to climate monitoring, and the approach assumes stationarity in

the relationship between temperature and precipitation variations across the region. It is therefore worth considering whether the non-stationarity of the climate would impact the value of the network under climate change. The approach uses the covariance structure to identify optimal observing locations, which is primarily affected by terrain features: elevation, aspect, proximity to the coast, etc. Since these will not change with a changing climate – future storms will still come from the west, temperatures in the interior will still be more variable than at the coasts, etc. – we do not believe that this is a major concern. Furthermore, the assumption that the statistical relationships will remain the same with a changing climate is common in climate research (e.g., statistical downscaling, paleoclimate reconstructions). Moreover, an alternative approach, such as using GCM simulations, would have its own set of caveats in this regard (e.g., bias, coarse resolution, etc.).

A primary advantage of the ensemble sensitivity method is that it can be modified in a way that takes into account practical and scientific considerations while ensuring that the network maximizes return on investment. For instance, there are important practical constraints on station siting, such as land ownership, proximity to roads, and the presence of existing stations. These are easily incorporated into the calculations by (a) constraining the first "n" station selections to correspond to existing observations, and (b) simply masking out grid cells that do not conform to certain criteria. Furthermore, climatological networks are not designed to monitor just one quantity, and it is not necessarily the case that sites that capture a large fraction of the variance in precipitation should also be useful for monitoring other variables. The method could be made to iteratively select temperature and precipitation stations, making each conditional on the other. Flexibility is a key advantage of this approach: it can be easily adapted to the practical constraints of station siting while still ensuring that the monitoring goals are pursued optimally.

There are numerous potential applications for the ensemble sensitivity method spanning multiple fields, monitoring goals, and regions of interest. The advantage of optimal design is that it ensures an efficient use of resources. We believe that this approach can be a useful tool for informing decisions in network design.

Acknowledgements. Funding for this research was provided in part by NSF Grant 1043090, as well as the State of Washington through funding to the Office of Washington State Climatologist.

References

Abatzoglou, J., Redmond, K., and Edwards, L.: Classification of regional climate variability in the state of California, J. Appl. Meteorol., 48, 1527–1541, http://dx.doi.org/10.1175/2009JAMC2062.1, 2009.

Alfonso, L., Lobbrecht, A., and Price, R.: Optimization of water level monitoring network in polder systems using information theory, Water Resour. Res., 46, W12553, http://dx.doi.org/10.1029/2009WR008953, 2010.

Ancell, B. and Hakim, G.: Comparing Adjoint-and Ensemble-Sensitivity Analysis with Applications to Observation Targeting, Mon. Weather Rev., 135, 4117–4134, http://dx.doi.org/10.1175/2007MWR1904.1, 2007.

Bergot, T., Hello, G., Joly, A., and Malardel, S.: Adaptive Observations: A Feasibility Study, Mon. Weather Rev., 127, 743–765, 1999.

Bishop, C. and Toth, Z.: Ensemble transformation and adaptive observations, J. Atmos. Sci., 56, 1748–1765, http://dx.doi.org/10.1175/1520-0469(1999)056⟨1748:ETAAO⟩2.0.CO;2, 1999.

Creelman, C. and Risk, D.: Network design for soil CO_2 monitoring of the northern North American region, Ecol. Modell., 222, 3421–3428, 2011.

Dabberdt, W. and Schlatter, T.: Research opportunities from emerging atmospheric observing and modeling capabilities, B. Am. Meteorol. Soc., 77, 305–323, 1996.

Daly, C., Gibson, W., Taylor, G., Johnson, G., and Pasteris, P.: A knowledge-based approach to the statistical mapping of climate, Clim. Res., 22, 99–113, 2002.

Dixon, W. and Chiswell, B.: Review of aquatic monitoring program design, Water Res., 30, 1935–1948, 1996.

Fuentes, M., Chaudhuri, A., and Holland, D. M.: Bayesian entropy for spatial sampling design of environmental data, Environ. Ecol. Stat., 14, 323–340, http://dx.doi.org/10.1007/s10651-007-0017-0, 2007.

Fujioka, F.: A method for designing a fire weather network, J. Atmos. Ocean. Technol., 3, 564–570, 1986.

Hamill, T.: Ensemble-based atmospheric data assimilation, 124–156, Cambridge Univ. Press, New York, 2006.

Hargrove, W., Hoffman, F., and Law, B.: New analysis reveals representativeness of the AmeriFlux network, Eos, 84, 529–535, 2003.

Huntley, H. and Hakim, G.: Assimilation of time-averaged observations in a quasi-geostrophic atmospheric jet model, Clim. Dynam., 35, 995–1009, http://dx.doi.org/10.1007/s00382-009-0714-5, 2010.

Kalman, R.: A new approach to linear filtering and prediction problems, J. Basic Eng., 82, 35–45, 1960.

Khare, S. and Anderson, J.: A methodology for fixed observational network design: theory and application to a simulated global prediction system, Tellus A, 58, 523–537, 2006.

Kurdzo, J. and Palmer, R.: Objective Optimization of Weather Radar Networks for Low-Level Coverage Using a Genetic Algorithm, J. Atmos. Ocean. Technol., 29, 807–821, 2012.

Lawrimore, J. H., Menne, M. J., Gleason, B. E., Williams, C. N., Wuertz, D. B., Vose, R. S., and Rennie, J.: An overview of the Global Historical Climatology Network monthly mean temperature data set, version 3, Journal of Geophysical Research: Atmospheres (1984–2012), 116, 2011.

Lundquist, J. and Cayan, D.: Surface temperature patterns in complex terrain: Daily variations and long-term change in the central Sierra Nevada, California, J. Geophys. Res., 112, D11124, http://dx.doi.org/10.1029/2006JD007561, 2007.

Mesinger, F., DiMego, G., Kalnay, E., Mitchell, K., Shafran, P., Ebisuzaki, W., Jovic, D., Woollen, J., Rogers, E., Berbery, E., Ek, M., Fan, Y., Grumbine, R., Higgins, W., Li, H., Lin, Y., Manikin, G., Parrish, D., and Shi, W.: North American regional reanalysis, B. Am. Meteorol. Soc., 87, 343–360, http://dx.doi.org/10.

1175/BAMS-87-3-343, 2006.

Mishra, A. and Coulibaly, P.: Developments in hydrometric network design: A review, Rev. Geophys., 47, RG2001, http://dx.doi.org/10.1029/2007RG000243, 2009.

Morss, R., Emanuel, K., and Snyder, C.: Idealized adaptive observation strategies for improving numerical weather prediction, J. Atmos. Sci., 58, 210–232, 2001.

Nychka, D. and Saltzman, N.: Design of Air-Quality Monitoring Networks, 51–76, Springer-Verlag, New York, 1998.

Potter, J. E.: W matrix augmentation, M.I.T. Instrumentation Laboratory Memo SGA 5-64, Massachusetts Institute of Technology, Cambridge, MA, 1964.

Volkmann, T., Lyon, S., Gupta, H., and Troch, P.: Multicriteria design of rain gauge networks for flash flood prediction in semiarid catchments with complex terrain, Water Resour. Res., 46, W11554, http://dx.doi.org/10.1029/2010WR009145, 2010.

Wu, L. and Bocquet, M.: Optimal redistribution of the background ozone monitoring stations over France, Atmos. Environ., 45, 772–783, 2011.

Table 1. Meteorological datasets used.

Dataset	Resolution	Notes
PRISM: Parameter-elevation Regressions on Independent Slopes Model	2.5 arc-min (∼4 km)	Daly et al. (2002)
NARR: North American Regional Reanalysis	32 km	Mesinger et al. (2006)
GHCN: Global Historical Climatology Network, v 3.0	N/A (point observations)	Lawrimore et al. (2011)

Table 2. Statistics of annual climate data for both temperature and precipitation. Results for precipitation are shown for both the raw data and after the tranformation to Gaussian, as described in the text. For each statistic, the median for all grid cells is listed followed by the 5th and 95th percentile values in parentheses. Note that a Gaussian distribution has a skewness of 0 and a kurtosis of 3, but that with smaller sample sizes a discrete approximation to a Gaussian results in slightly lower values for the kurtosis.

Variable	Source	Mean	Variance	Skewness	Kurtosis
Temperature (°C)	GHCN	10.1 (5.2, 12.3)	0.5 (0.3, 1.2)	−0.4 (−1.5, 0.3)	3.2 (2.2, 6.2)
	PRISM	6.9 (2.0, 11.2)	0.6 (0.3, 1.2)	−0.1 (−0.7, 0.5)	2.8 (2.3, 4.1)
	NARR	7.8 (2.2, 11.9)	0.6 (0.2, 1.1)	−0.1 (−0.7, 0.3)	2.7 (2.0, 4.0)
Raw Precip ($m\,yr^{-1}$)	GHCN	0.59 (0.23, 2.1)	0.016 (0.0039, 0.21)	0.6 (−0.1, 2.0)	3.0 (2.0, 8.4)
	PRISM	0.53 (0.24, 2.3)	0.010 (0.0034, 0.16)	0.4 (−0.1, 1.0)	3.0 (2.2, 4.8)
	NARR	0.56 (0.26, 1.9)	0.015 (0.0043, 0.17)	0.5 (−0.2, 1.1)	2.8 (2.0, 4.3)
Transformed Precip	GHCN	0 (0, 0)	0.015 (0.0036, 0.20)	0 (0, 0)	2.5 (2.5, 2.5)
	PRISM	0 (0, 0)	0.010 (0.0033, 0.15)	0 (0, 0)	2.7 (2.7, 2.7)
	NARR	0 (0, 0)	0.014 (0.0043, 0.16)	0 (0, 0)	2.5 (2.5, 2.5)

Fig. 1. Map of the study region, defined as the region encompassed by the US states of Idaho, Oregon, and Washington. The map and legend highlight several geographic features as well as the cities of Boise, Portland, and Seattle. The color scale shows elevation above sea level in meters.

Table 4: GHCN station attributes.

ID	Latitude	Longitude	Elevation (m)	U.S. State	Station Name	Notes
USC00100010	42.9536	-112.8253	1342.6	ID	ABERDEEN EXP STN	HCN*
USC00100667	47.9803	-116.5594	636.1	ID	BAYVIEW MODEL BASIN	
USC00101017	43.7383	-116.2022	1184.1	ID	BOISE 7 N	
USC00101018	43.5253	-116.0542	865.6	ID	BOISE LUCKY PEAK DAM	
USC00101220	42.6006	-114.7453	1158.2	ID	BUHL #2	
USC00101363	48.0864	-116.0572	662.3	ID	CABINET GORGE	
USC00101408	44.5733	-116.6753	807.7	ID	CAMBRIDGE	HCN
USC00101514	44.5228	-116.0481	1492.3	ID	CASCADE 1 NW	
USC00101551	42.5503	-114.8661	1165.9	ID	CASTLEFORD 2 N	
USC00101671	43.9772	-113.8289	1908.0	ID	CHILLY BARTON FLAT	
USC00102260	43.4650	-113.5581	1797.4	ID	CRATERS OF THE MOON	
USC00102444	43.5764	-116.7475	765.0	ID	DEER FLAT DAM	
USC00102707	44.2436	-112.2006	1661.2	ID	DUBOIS EXP STN	
USC00102845	46.5022	-116.3217	303.3	ID	DWORSHAK FISH HATCH	HCN
USC00102875	45.8356	-115.4611	1236.9	ID	ELK CITY 1NE	
USC00102942	43.8544	-116.4664	728.5	ID	EMMETT 2 E	
USC00103143	46.0931	-115.5356	475.5	ID	FENN RS	HCN
USC00103297	43.0428	-112.4133	1360.9	ID	FT HALL 1 NNE	
USC00103631	42.9403	-115.3231	751.6	ID	GLENNS FERRY	HCN
USC00103771	45.9414	-116.1175	1005.8	ID	GRANGEVILLE	
USC00103964	43.9664	-112.2642	1460.0	ID	HAMER 4 NW	
USC00104140	42.5972	-114.1378	1237.5	ID	HAZELTON	HCN
USC00104295	42.3528	-114.5739	1379.2	ID	HOLLISTER	HCN
USC00104384	43.7828	-113.0033	1469.1	ID	HOWE	
USC00104442	43.8383	-115.8319	1208.5	ID	IDAHO CITY	
USC00104456	43.3456	-111.7847	1776.4	ID	IDAHO FALLS 16 SE	
USC00104670	42.7325	-114.5192	1140.0	ID	JEROME	HCN
USC00104831	47.5339	-116.1222	724.5	ID	KELLOGG	HCN
USC00104845	43.6842	-114.3603	1795.3	ID	KETCHUM RS	HCN
USC00105275	42.1231	-111.3139	1806.2	ID	LIFTON PUMPING STN	HCN
USC00105708	44.8872	-116.1047	1531.6	ID	MC CALL	
USC00105897	44.7189	-115.0150	1365.5	ID	MIDDLE FORK LODGE	
USC00106152	46.7281	-116.9558	810.8	ID	MOSCOW U OF I	HCN
USC00106305	43.6039	-116.5753	752.9	ID	NAMPA SUGAR FACTORY	HCN
USC00106542	42.2342	-113.8981	1389.6	ID	OAKLEY	HCN
USC00106844	43.8022	-116.9442	698.0	ID	PARMA EXP STN	
USC00106891	44.0764	-116.9311	655.3	ID	PAYETTE	HCN
USC00107040	43.3111	-114.0742	1472.2	ID	PICABO	
USC00107046	46.4922	-115.8006	938.8	ID	PIERCE	
USC00107320	46.5100	-114.7111	1075.9	ID	POWELL	
USC00107386	48.3511	-116.8353	722.7	ID	PRIEST RIVER EXP STN	HCN
USC00107648	43.2064	-116.7494	1197.9	ID	REYNOLDS	
USC00108022	43.9517	-111.6789	1496.6	ID	SAINT ANTHONY	
USC00108080	45.1875	-113.9008	1198.2	ID	SALMON-KSRA	HCN
USC00108380	42.9383	-114.4169	1204.0	ID	SHOSHONE 1 WNW	
USC00108928	43.2436	-116.3783	708.7	ID	SWAN FALLS P H	
USC00108937	43.4447	-111.2939	1633.7	ID	SWAN VALLEY 2 E	
USC00109065	43.8564	-111.2769	1880.6	ID	TETONIA EXP STN	
USC00109303	42.5458	-114.3461	1207.0	ID	TWIN FALLS 6 E	
USC00109846	46.2381	-116.6233	1210.7	ID	WINCHESTER	
USC00350304	42.2128	-122.7144	532.2	OR	ASHLAND	HCN
USC00350471	43.1497	-124.4019	6.1	OR	BANDON 2 NNE	

continued on next page...

ID	Latitude	Longitude	Elevation (m)	U.S. State	Station Name	Notes
USC00350652	44.2867	-122.0386	655.9	OR	BELKNAP SPRINGS 8 N	
USC00350694	44.0567	-121.2850	1115.6	OR	BEND	HCN
USC00350897	45.6361	-121.9519	18.9	OR	BONNEVILLE DAM	
USC00351433	44.3914	-122.4811	292.6	OR	CASCADIA	HCN
USC00351448	42.1597	-123.6422	419.7	OR	CAVE JUNCTION 1 WNW	
USC00351643	46.1081	-123.2058	6.7	OR	CLATSKANIE	
USC00351765	45.2325	-120.1817	865.6	OR	CONDON	HCN
USC00351836	43.1872	-124.2025	7.0	OR	COQUILLE CITY	
USC00351862	44.6342	-123.1900	68.6	OR	CORVALLIS STATE UNIV	HCN
USC00351877	44.5078	-123.4575	180.4	OR	CORVALLIS WATER BUREAU	
USC00351902	43.7178	-123.0578	253.3	OR	COTTAGE GROVE DAM	
USC00351946	42.8967	-122.1328	1973.6	OR	CRATER LAKE NPS HQ	HCN
USC00352112	44.9464	-123.2908	88.4	OR	DALLAS 2 NE	
USC00352173	44.5564	-119.6447	688.8	OR	DAYVILLE 8 NW	
USC00352292	44.7242	-122.2547	371.9	OR	DETROIT DAM	
USC00352406	43.6656	-123.3275	89.0	OR	DRAIN	HCN
USC00352693	45.2689	-122.3186	137.2	OR	ESTACADA 2 SE	
USC00353047	44.4139	-122.6728	167.6	OR	FOSTER DAM	
USC00353356	42.4036	-124.4242	15.2	OR	GOLD BEACH RS	
USC00353402	45.3014	-121.7417	1213.1	OR	GOVERNMENT CAMP	
USC00353692	42.5483	-119.6556	1711.8	OR	HART MTN REFUGE	
USC00353770	45.4486	-122.1547	228.0	OR	HEADWORKS PORTLAND WTR	HCN
USC00353827	45.3653	-119.5639	574.5	OR	HEPPNER	HCN
USC00353995	43.9281	-124.1069	35.1	OR	HONEYMAN SP	
USC00354003	45.6847	-121.5175	152.4	OR	HOOD RIVER EXP STN	HCN
USC00354126	43.3708	-122.9653	329.2	OR	IDLEYLD PARK 4 NE	
USC00354291	44.4233	-118.9594	933.6	OR	JOHN DAY	
USC00354606	44.6253	-122.7189	158.5	OR	LACOMB 3 NNE	
USC00354622	45.3167	-118.0747	839.7	OR	LA GRANDE	
USC00354811	44.1014	-122.6886	205.7	OR	LEABURG 1 SW	
USC00354835	43.3597	-122.2208	1242.7	OR	LEMOLO LAKE 3 NNW	
USC00355050	43.9144	-122.7600	217.0	OR	LOOKOUT POINT DAM	
USC00355055	42.6722	-122.6750	481.6	OR	LOST CREEK DAM	
USC00355142	44.6633	-121.1461	744.6	OR	MADRAS 2 N	
USC00355160	43.9794	-117.0247	688.8	OR	MALHEUR BRANCH EXP STN	
USC00355221	44.6125	-121.9486	754.4	OR	MARION FRKS FISH HATCH	
USC00355593	45.9428	-118.4089	295.7	OR	MILTON FREEWATER	HCN
USC00355711	44.8186	-119.4200	608.1	OR	MONUMENT 2	
USC00355734	45.4825	-120.7236	570.0	OR	MORO	HCN
USC00356179	43.8764	-116.9903	662.9	OR	NYSSA	
USC00356213	43.7428	-122.4433	388.6	OR	OAKRIDGE FISH HATCHERY	
USC00356334	45.3558	-122.6047	50.9	OR	OREGON CITY	
USC00356366	45.0333	-123.9239	45.7	OR	OTIS 2 NE	
USC00356405	43.6500	-117.2467	731.5	OR	OWYHEE DAM	
USC00356532	44.7275	-121.2506	429.8	OR	PELTON DAM	
USC00356784	42.7519	-124.5011	12.8	OR	PORT ORFORD NO 2	
USC00356907	42.7342	-122.5164	756.5	OR	PROSPECT 2 SW	HCN
USC00357169	42.9506	-123.3572	207.3	OR	RIDDLE	HCN
USC00357277	43.3636	-117.1142	1118.6	OR	ROCKVILLE 5 N	
USC00357331	43.2131	-123.3658	129.5	OR	ROSEBURG KQEN	HCN
USC00357641	45.9869	-123.9236	3.0	OR	SEASIDE	
USC00357675	44.1383	-118.9750	1420.4	OR	SENECA	
USC00357817	43.1244	-121.0620	1335.6	OR	SILVER LAKE RS	
USC00357823	45.0058	-122.7739	124.4	OR	SILVERTON	

continued on next page...

ID	Latitude	Longitude	Elevation (m)	U.S. State	Station Name	Notes
USC00358095	44.7892	-122.8142	129.5	OR	STAYTON	
USC00358173	42.9592	-120.7897	1277.7	OR	SUMMER LAKE 1 S	
USC00358536	43.2750	-122.4497	627.9	OR	TOKETEE FALLS	
USC00358797	43.9814	-117.2439	682.8	OR	VALE	HCN
USC00358884	45.8653	-123.1903	190.5	OR	VERNONIA NO 2	
USC00359316	43.6825	-121.6875	1328.3	OR	WICKIUP DAM	
USC00450008	46.9658	-123.8292	3.0	WA	ABERDEEN	HCN
USC00450482	45.7717	-122.5286	86.6	WA	BATTLE GROUND	
USC00450844	48.9947	-117.3544	559.9	WA	BOUNDARY DAM	
USC00450945	47.1694	-122.0036	208.8	WA	BUCKLEY 1 NE	HCN
USC00451276	46.7200	-122.9528	56.4	WA	CENTRALIA	HCN
USC00451350	47.8361	-120.0381	335.0	WA	CHELAN	
USC00451400	47.9967	-119.6483	254.2	WA	CHIEF JOSEPH DAM	
USC00451484	48.9672	-122.3292	19.5	WA	CLEARBROOK	HCN
USC00451767	47.9544	-118.9997	524.0	WA	COULEE DAM 1 SW	
USC00451939	47.3706	-123.1600	6.4	WA	CUSHMAN POWERHOUSE 2	HCN
USC00452007	47.6575	-118.1614	722.1	WA	DAVENPORT	HCN
USC00452157	48.7142	-121.1431	271.6	WA	DIABLO DAM	
USC00452505	46.9692	-120.5400	451.1	WA	ELLENSBURG	HCN
USC00452531	47.0092	-123.4008	21.3	WA	ELMA	
USC00452548	48.0164	-123.5906	109.7	WA	ELWHA RS	
USC00452675	47.9753	-122.1950	18.3	WA	EVERETT	HCN
USC00452914	47.9558	-124.3539	106.7	WA	FORKS 1 E	HCN
USC00453515	47.4933	-118.2500	658.4	WA	HARRINGTON 1 NW	
USC00453883	46.2447	-118.8786	112.2	WA	ICE HARBOR DAM	
USC00454154	46.2111	-119.1011	118.9	WA	KENNEWICK	HCN
USC00454338	46.8167	-117.8831	449.9	WA	LACROSSE	
USC00454679	47.0022	-118.5658	496.8	WA	LIND 3 NE	
USC00454748	46.3675	-124.0378	7.6	WA	LONG BEACH EXP STN	HCN
USC00454764	46.7492	-121.8120	841.9	WA	LONGMIRE RAINIER NPS	HCN
USC00454769	46.1506	-122.9164	3.7	WA	LONGVIEW	HCN
USC00455224	47.1358	-122.2558	176.5	WA	MC MILLIN RSVR	HCN
USC00455704	47.1414	-121.9356	398.7	WA	MUD MTN DAM	
USC00456039	47.3328	-118.6944	470.0	WA	ODESSA	HCN
USC00456096	48.6117	-122.8064	24.4	WA	OLGA 2 SE	HCN
USC00456262	46.6092	-121.6744	323.1	WA	PACKWOOD	
USC00456295	47.3058	-121.8514	280.4	WA	PALMER 3 ESE	
USC00456534	47.7850	-120.6456	590.1	WA	PLAIN	
USC00456789	46.7603	-117.1861	766.6	WA	PULLMAN 2 NW	HCN
USC00456846	47.8092	-122.9136	37.5	WA	QUILCENE 2 SW	
USC00456880	47.2156	-119.8478	388.3	WA	QUINCY 1 S	
USC00456898	46.7858	-121.7425	1654.1	WA	RAINIER PARADISE RS	
USC00456974	48.6469	-118.7314	798.6	WA	REPUBLIC	
USC00457059	47.1178	-118.3722	566.9	WA	RITZVILLE 1 SSE	HCN
USC00457180	47.2325	-117.3625	733.0	WA	ROSALIA	
USC00457185	48.7272	-121.0722	376.7	WA	ROSS DAM	
USC00457267	47.0933	-117.5878	595.0	WA	ST. JOHN	HCN
USC00457507	48.4958	-122.2355	18.3	WA	SEDRO WOOLLEY	HCN
USC00457696	45.6228	-122.2175	134.1	WA	SKAMANIA FISH HATCHRY	
USC00458773	45.6778	-122.6511	64.0	WA	VANCOUVER 4 NNE	HCN
USC00459200	46.0436	-118.4628	192.6	WA	WHITMAN MISSION	
USC00459376	48.4742	-120.1886	533.1	WA	WINTHROP 1 WSW	HCN
USW00024130	44.8428	-117.8086	1024.4	OR	BAKER CITY MUNI AP	HCN
USW00024131	43.5667	-116.2406	857.7	ID	BOISE AIR TERMINAL	GSN**, WMO 72681***

continued on next page...

ID	Latitude	Longitude	Elevation (m)	U.S. State	Station Name	Notes
USW00024133	42.5417	-113.7661	1262.5	ID	BURLEY MUNI AP	
USW00024141	47.3078	-119.5153	381.6	WA	EPHRATA MUNI AP	WMO 72790
USW00024149	46.3747	-117.0156	437.7	ID	LEWISTON NEZ PERCE CO AP	HCN, WMO 72783
USW00024155	45.6906	-118.8528	461.8	OR	PENDLETON	GSN, WMO 72688
USW00024156	42.9203	-112.5711	1364.9	ID	POCATELLO RGNL AP	GSN, WMO 72578
USW00024157	47.6217	-117.5281	717.2	WA	SPOKANE INTL AP	HCN, WMO 72785
USW00024162	44.0206	-117.0128	667.5	OR	ONTARIO MUNI AP	
USW00024219	45.6194	-121.1661	71.6	WA	THE DALLES MUNI AP	
USW00024221	44.1278	-123.2206	107.6	OR	EUGENE MAHLON SWEET AP	WMO 72693
USW00024225	42.3811	-122.8722	395.3	OR	MEDFORD ROGUE VLY AP	WMO 72597
USW00024227	46.9733	-122.9033	57.3	WA	OLYMPIA AP	GSN, WMO 72792
USW00024229	45.5908	-122.6003	5.8	OR	PORTLAND INTL AP	WMO 72698
USW00024232	44.9050	-123.0011	62.5	OR	SALEM MCNARY FLD	WMO 72694
USW00024233	47.4444	-122.3139	112.8	WA	SEATTLE TACOMA INTL AP	WMO 72793
USW00024242	45.5511	-122.4089	8.8	OR	PORTLAND TROUTDALE AP	
USW00024243	46.5683	-120.5428	324.3	WA	YAKIMA AIR TERMINAL	WMO 72781
USW00024284	43.4133	-124.2436	5.2	OR	NORTH BEND RGNL AP	HCN
USW00094224	46.1569	-123.8825	2.7	OR	ASTORIA RGNL AP	HCN, WMO 72791
USW00094225	46.9728	-123.9303	3.7	WA	HOQUIAM BOWERMAN AP	
USW00094239	47.3978	-120.2014	374.6	WA	WENATCHEE PANGBORN AP	
USW00094240	47.9375	-124.5550	56.4	WA	QUILLAYUTE STATE AP	WMO 72797

* indicates the station is included in the U.S. Historical Climatology Network (HCN)

** indicates the station is included in the Global Climate Observing System (GCOS) Surface Network (GSN)

*** denotes the Word Meteorological Organization (WMO) number for the station

Table 3. Percent of the variance explained with each station selection. Values shown are the median and 5th–95th percentile values (in parentheses) based on all 50 000 Monte Carlo calculations.

Station #	Variance Explained (%)	
	Temperature	Precipitation
01	86.68 (82.18–89.57)	88.08 (83.50–91.21)
02	6.71 (05.00–09.30)	6.70 (04.20–11.08)
03	2.36 (01.68–03.41)	2.72 (01.62–04.38)
04	1.13 (00.80–01.66)	1.23 (00.69–02.18)
05	0.66 (00.47–00.97)	0.65 (00.36–01.22)
06	0.43 (00.31–00.63)	0.39 (00.21–00.74)
07	0.30 (00.22–00.44)	0.25 (00.13–00.48)
08	0.22 (00.16–00.32)	0.16 (00.08–00.32)
09	0.17 (00.13–00.25)	0.11 (00.06–00.22)
10	0.14 (00.10–00.19)	0.08 (00.04–00.16)
11	0.11 (00.08–00.16)	0.06 (00.03–00.12)
12	0.09 (00.07–00.13)	0.05 (00.02–00.09)
13	0.08 (00.06–00.11)	0.04 (00.02–00.07)
14	0.06 (00.05–00.09)	0.03 (00.01–00.06)
15	0.06 (00.04–00.08)	0.02 (00.01–00.05)
16	0.05 (00.04–00.07)	0.02 (00.01–00.04)
17	0.04 (00.03–00.06)	0.02 (00.01–00.03)
18	0.04 (00.03–00.05)	0.01 (00.01–00.03)
19	0.03 (00.03–00.05)	0.01 (00.01–00.03)
20	0.03 (00.02–00.04)	0.01 (00.00–00.02)

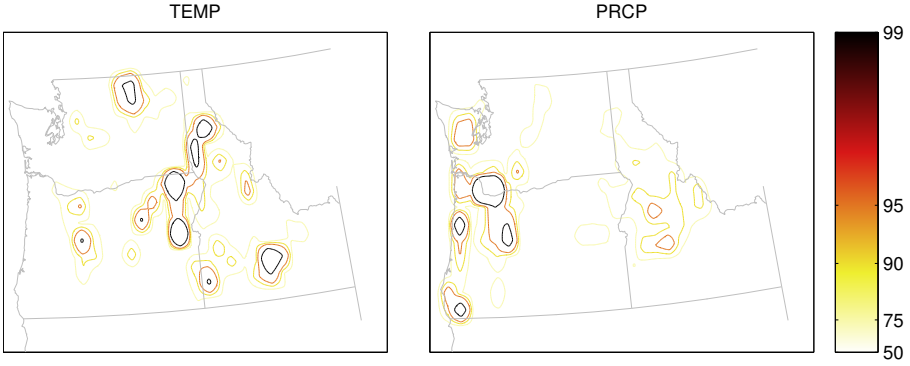

Fig. 2. Results for annual temperature and precipitation, obtained using the optimal network design calculation. Calculations were performed using regionally-averaged temperature and precipitation as the target metric (defined as the average over the US states of Idaho, Oregon, and Washington). Contours show the percentile value of the grid cell weighting – higher weights denote areas where measurements contribute more to the variance explained. Results are obtained using the PRISM dataset (1948–2011), central estimates for the measurement error (R^2), and a sample size of 30 yr.

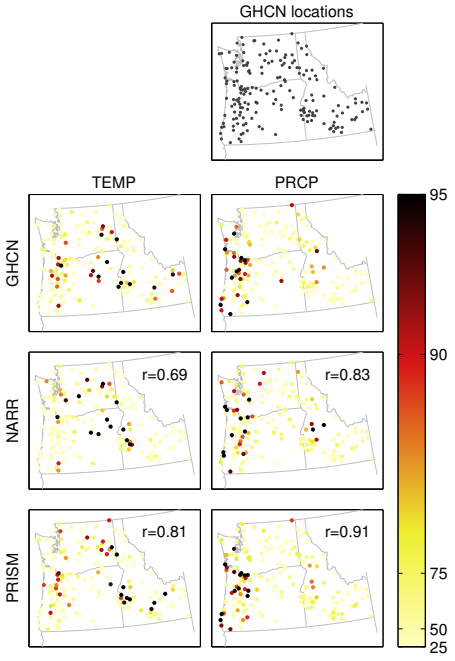

Fig. 3. Results from three different datasets (GHCN, NARR, PRISM), calculated for the 181 GHCN stations with continuous records for the period 1979–2011. The top map, labeled "GHCN locations", shows the location of the GHCN stations used in the calculation. The 6 other maps show results for the different datasets. Each dot denotes the location of a GHCN station, and is shaded according to the percentage of time the station was chosen using the network design algorithm. Rank correlations with the GHCN results are shown in the top right corner of the NARR and PRISM maps. As with Fig. 2, percentile values are plotted to simplify interpretation. Note that, unlike in other figures, the color scale remains a light yellow at low values, and does not fade to white.

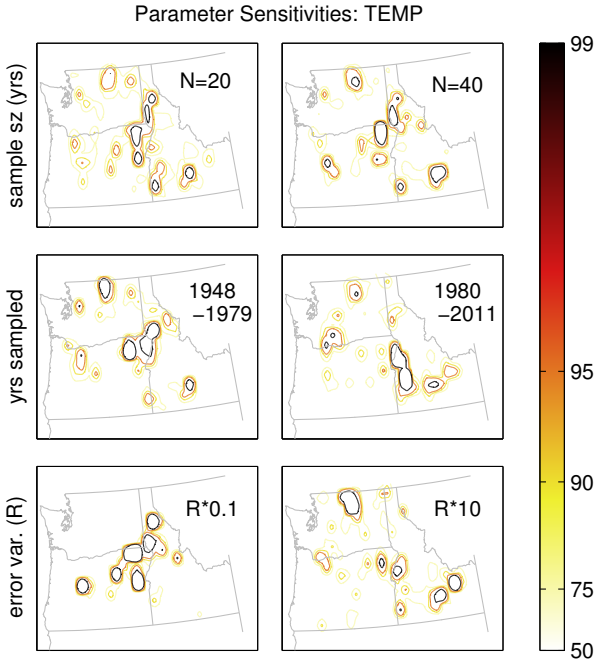

Fig. 4. Sensitivity of network design results for annual temperature, obtained by varying the parameters used to apply the algorithm. The top row shows results in which the sample size is varied between 20 and 40 yr, the middle row shows results obtained from the first half of the record (1948–1979) and the last half (1980–2011), and the bottom row shows the impact of scaling the measurement error (R^2) by an order of magnitude in each direction.

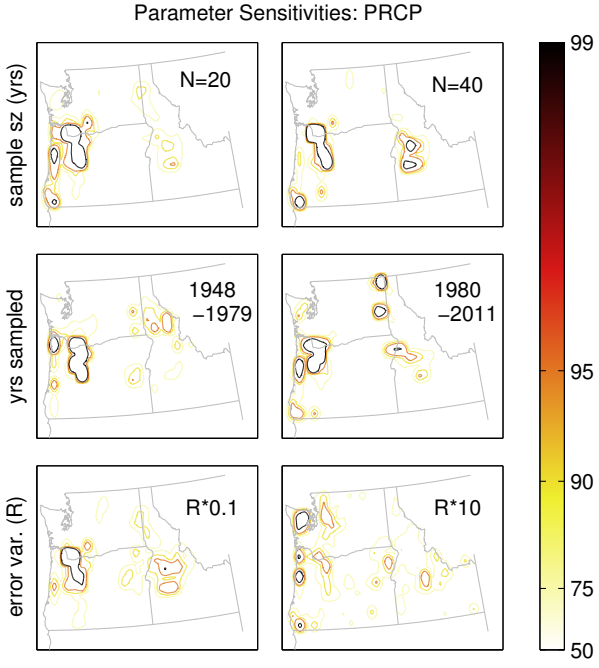

Fig. 5. As in Fig. 4 except applied to annual precipitation.